Resonant shifts of positronium energy levels in MgO powder

L. Gurung, B. S. Cooper, S. D. Hogan, and D. B. Cassidy ⬤

Department of Physics and Astronomy, University College London, Gower Street, London WC1E 6BT, United Kingdom

We report measurements of shifts in the frequencies of $1\,^3S_1 \to 2\,^3P_J$ and $2\,^3P_J \to n\,^3D/n\,^3S$ transitions optically driven in positronium atoms while they are inside the open volumes of MgO smoke powder. The observed intervals are larger than the corresponding vacuum excitations, but, surprisingly, the transitions to Rydberg states are less strongly affected, and the energy shifts exhibit no dependence on the principal quantum number n of the final state. We attribute these shifts to resonant interactions between Ps atoms and MgO surfaces, mediated via spectrally overlapping MgO ultra violet (UV) photo-luminescent absorption bands. Since many insulating materials suitable for Ps confinement exhibit similar broadband UV absorption characteristics, the observed phenomena have implications for optical diagnostics and laser cooling schemes of relevance to studies of high-density Ps ensembles in insulating cavities, including the production of a Ps Bose-Einstein condensate.

I. INTRODUCTION

The ability to cool and trap atoms (e.g., Refs. [1–3]) has opened the door to new regimes of atomic physics experiments, including studies of cold atom collisions [4], spectroscopy [5], and the observation of Bose-Einstein condensation (BEC) [6]. Thermal atoms can be laser-cooled to mK temperatures, allowing them to be loaded into optical or electromagnetic traps where other techniques, such as evaporative cooling [7], can be applied to reduce the temperature further. This method was used to achieve the first BEC of alkali metal atoms [8], and since that time condensates have been produced via several other techniques, including buffer gas cooling [9] and direct laser cooling [10]. Many species can now be Bose condensed, including atomic hydrogen [11].

Positronium (Ps) is a hydrogenic atom composed of a positron-electron bound state. Since electrons and positrons are both fermions, the composite Ps is a bosonic system. A long-term goal of positronium physics is to observe BEC in this system [12,13]. This is a necessary prerequisite to the observation of stimulated annihilation [14–16], and Bose-condensed Ps would provide an ideal source for Ps matter-wave interferometry [17]. Because of its low mass, the transition temperature T_c at which a dense ensemble of bosonic atoms will begin to condense [18] is much higher for Ps than it is for any other atomic system at the same density. For example, at a density of 10^{18} cm^{-3}, T_c is on the order of 15 K for Ps and 15 mK for hydrogen. However, the techniques that have previously been used to achieve BEC cannot easily be applied to Ps atoms. In particular, laser cooling of Ps [12] is complicated by its finite ground state lifetime (≈ 142 ns [19]) and the fact that Ps atoms generally move very fast [20].

Ps atoms can be produced within isolated cavities in some materials, which can therefore act as Ps traps [21]. This may at first seem counterintuitive, since interactions with solid matter can lead to annihilation. However, the rate at which Ps atoms decay following wall collisions can be much lower

than the intrinsic decay rate[1] for sufficiently large confining volumes, and for cavity diameters on the order of 100 nm, ground-state Ps lifetimes are essentially the same as in vacuum [23]. Thus, because T_c can conceivably be achieved via collisional thermalization for experimentally achievable densities, Ps confinement in cooled solid-state cavities could provide a route towards BEC.

Platzman and Mills have outlined a method to produce a Ps condensate in this way [13]; they suggested that a brightness-enhanced positron beam could be implanted into a cooled cavity so as to produce a dense Ps ensemble in which Ps-wall collisions will permit fast thermalization. Recent numerical simulations indicate that this can occur on a timescale that is compatible with the ground state triplet lifetime in cavities with diameters on the order of a few hundred nanometers [24]. However, introducing Ps atoms into such small volumes is technically challenging, requiring an unrealistically bright positron beam [25] or some sort of Ps collection scheme [26]. Producing Ps atoms in larger micron-scale cavities is more feasible from a practical point of view but would necessarily reduce the Ps cooling rate [27].

In order to experimentally implement some version of the Platzman-Mills scheme [13] it would be necessary to simultaneously optimize the Ps density and cooling in various target structures, which would require advanced diagnostics and perhaps, also, laser cooling. The latter has not been demonstrated, although simulations suggest that it is possible [28]. Laser cooling of confined Ps would have the advantage that the atoms are localized to a small volume, but in this case line-narrowing effects [29–31] due to Ps-surface and Ps-Ps scattering would have to be properly taken into account, for example by using short laser pulses or coherent excitation

---

[1]This is the case only for insulating cavities; the free electrons in metals and semiconductors will lead to rapid annihilation or spin flipping to short-lived states, as will the presence of paramagnetic centers [22].

schemes [32,33]. For cold confined atoms, an optical measurement of the Ps density could be achieved by monitoring the $1\,^3S_1 \rightarrow 2\,^3S_1$ cold-collision frequency shift [34], which is particularly large in Ps at relevant densities [35]; a direct diagnostic of the Ps density that could be time resolved would be invaluable for target design and optimization.

We show here that optical probes or cooling schemes applied to Ps atoms confined in insulator cavities may be strongly affected by interactions between the atoms and the internal confining surfaces; measurements were performed in which Ps atoms created in large open internal volumes in MgO smoke powder were optically excited, with $1\,^3S_1 \rightarrow 2\,^3P_J$ and $2\,^3P_J \rightarrow n\,^3D/n\,^3S$ transitions driven using a two-color two-photon scheme [36,37]. Large shifts in the transition frequencies, on the order of terahertz, were observed when Ps atoms were probed while inside the internal spaces of an MgO powder target. We attribute these shifts to resonant interactions between Ps atoms and the broad (230–255 nm) photoluminescence (PL) absorption bands in MgO [38], which overlap with the 243-nm $1\,^3S_1 \rightarrow 2\,^3P_J$ transition.

II. EXPERIMENTAL METHODS

The experiments were performed using a positron beam and measurement techniques described elsewhere [39,40]. The general methodology is as follows: a pulsed positron beam was implanted into an MgO smoke powder target, producing Ps atoms [41]. These atoms were optically excited, and Ps lifetimes were monitored using gamma-ray detectors. By directing laser light into the target material or along its surface, Ps atoms could be probed either after they had been emitted into the vacuum or while they were still inside the MgO powder, as indicated in Figs. 1(a) and 1(b), respectively. Only the long-lived ground state (ortho-Ps) is studied in this work.

Two pulsed dye lasers (with pulse durations of 6 ns, FWHM) were used in the experiments; a UV laser ($\approx 500\ \mu$J/pulse, $\Delta\nu = 85$ GHz, $\lambda = 243$ nm) was used to drive $1\,^3S_1 \rightarrow 2\,^3P_J$ transitions in Ps, and a second simultaneous IR laser (≈ 10 mJ/pulse, $\Delta\nu = 5$ GHz, $\lambda \approx 729 - 760$ nm) was used to drive $2\,^3P_J \rightarrow n\,^3D/n\,^3S$ transitions or to photoionize $2\,^3P_J$ atoms.

Ps production and optical excitation was monitored via the time dependence of its annihilation gamma radiation [42]; when atoms were excited and immediately photoionized, the amount of long-lived Ps present was decreased. Conversely, if Rydberg states were generated, the amount of longer-lived Ps was increased. Thus lifetime spectra can be used to characterize optical Ps excitation. Ps annihilation radiation was monitored by fast gamma-ray detectors [40,43]. The amount of long-lived Ps present was parameterized by the quantity $f = \int_B^C V(t)\, \mathrm{d}t / \int_A^C V(t)\, \mathrm{d}t$, where A, B, and C define integration time windows, and $V(t)$ is the gamma-ray detector output voltage. For the work reported here, time windows $(A, B, C) = (-30, 40, 400)$ ns were used to observe photoionization events following $1\,^3S_1 \rightarrow 2\,^3P_J$ transitions, and $(A, B, C) = (-30, 200, 600)$ ns were used for Rydberg measurements (i.e., $1\,^3S_1 \rightarrow 2\,^3P_J \rightarrow n\,^3D/n\,^3S$). These windows were chosen to optimize the signal-to-noise ratio as
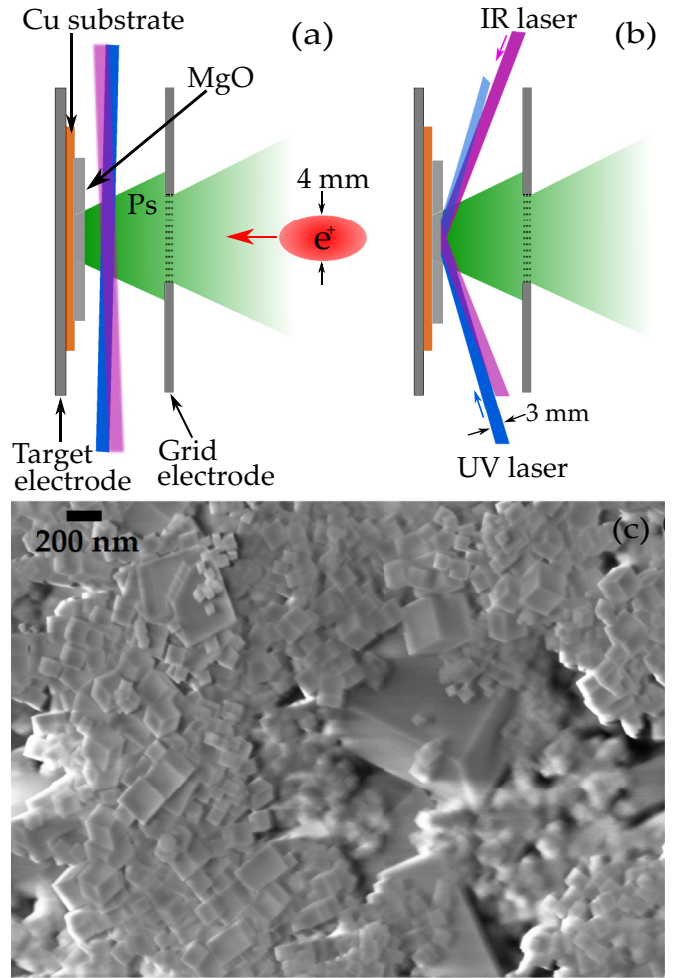

FIG. 1. Orientation of the lasers and target holder used to excite Ps atoms (a) in vacuum and (b) inside the MgO target. The (green) cone represents Ps emitted from the MgO powder into vacuum. (c) A Karl Zeiss XB1540 scanning electron microscopy (SEM) image of MgO smoke nanocrystals deposited on a Cu plate obtained with an electron-beam energy of 3 keV.

detailed in [40]. Different time windows are needed for the Rydberg atoms studied here because of their long lifetimes ($\geqslant 1\ \mu$s) arising from reduced electron-positron overlap [44]. Data were recorded for two cases, namely, with the excitation laser tuned on (Sig) and off (Back) resonance with the transition being studied. Laser-induced effects were characterized by the parameter $S_\gamma = (f_{\mathrm{Back}} - f_{\mathrm{Sig}})/f_{\mathrm{Back}}$ [39].

The MgO target was produced by burning a 10-cm-long piece of magnesium ribbon in air, and the smoke powder was collected on a clean copper substrate. MgO smoke powder consists of perfectly cubic $(1\,0\,0)$ nanocrystals [45] with edge lengths ranging from a few nanometers to microns [46]. This structure can be observed in Fig. 1(c), which shows an electron micrograph of an MgO target nominally identical to those used in the Ps measurements. Using IMAGEJ analysis software [47], we determined that the mean crystal edge length was 120 nm, with a broad distribution ranging from approximately 10 nm to 1 μm. We estimate the MgO layer thickness to be on the order of 30 μm [48].

The presence of even a small number of micron-size cubes means that the open spaces in the MgO powder may also be similarly large. In separate measurements [48] we have found that Ps atoms are able to travel through tens of microns of MgO powder without significant energy loss or annihilation, indicating that the internal spaces between crystals are large and interconnected. The lack of observed cooling can be used to set a lower limit of $\approx 1\,\mu m$ on the Ps mean free path between collisions, based on a collisional cooling model [49]. However, this model may not be applicable if there are strong Ps-surface interactions; since the measured MgO cube distribution extends up to $1\,\mu m$, we would not expect open volumes significantly larger than this to be present, and none are observed in scanning electron microscopy (SEM) images. Thus, MgO smoke powder acts as a convenient proxy for a confining insulator system on the submicron scale. Ps atoms can be probed while they remain in the internal volumes and interact with surfaces but can subsequently leave the sample and so can also be probed in vacuum. Henceforth we shall refer to both vacuum and confined Ps atoms with the understanding that atoms temporarily reside in the internal MgO voids but are not actually confined therein.

Ps atoms emitted from MgO nanocrystal surfaces have kinetic energies on the order of 350 meV [48], and the Ps-surface scattering rate ω_S (assuming a maximum $1\,\mu m$ mean free path) will therefore be at least 250 GHz while the atoms remain in the powder. For the laser parameters used in the present experiments, the Rabi frequency for $1\,^3S_1 \to 2\,^3P_J$ transitions ω_R is estimated to be on the order of 10 GHz (e.g., [50]), meaning that during the excitation process atoms will scatter from MgO surfaces multiple times. We note that the condition $\omega_S > \omega_R$ precludes the application of typical laser cooling schemes [51].

III. RESULTS AND DISCUSSION

Figure 2 shows spectra of the $1\,^3S_1 \to 2\,^3P_J$ transition driven in Ps atoms both in vacuum and inside the MgO sample using the laser configurations shown in Fig. 1. For these measurements the IR laser was tuned to 729 nm to photoionize $n = 2$ atoms. Measurements in which the lasers were directed into the target were both prompt and delayed, where prompt excitation means that the lasers were fired almost synchronously with the positron pulse, and delayed excitation includes a 10-ns laser delay. In the prompt case Ps atoms will be excited in the MgO and in vacuum. When the laser was delayed, however, fewer vacuum atoms were present, and a larger fraction of the observed signal corresponded to confined atoms.

Ps excitation in vacuum [Fig. 2(a)] shows a typical Doppler-broadened spectrum corresponding to atoms with a mean transverse kinetic energy of ≈ 350 meV, as has been observed in previous experiments using MgO powder targets [48]. To measure confined Ps the lasers were directed into the sample [Fig. 2(b)], and in this case two peaks were observed, one redshifted and one blueshifted. The separation of these peaks was more apparent for the delayed measurements [Fig. 2(c)]. The redshifted peak (i.e., shifted to longer wavelengths) arises from the interaction of Ps atoms in vacuum moving towards the incoming laser beam. Similarly,
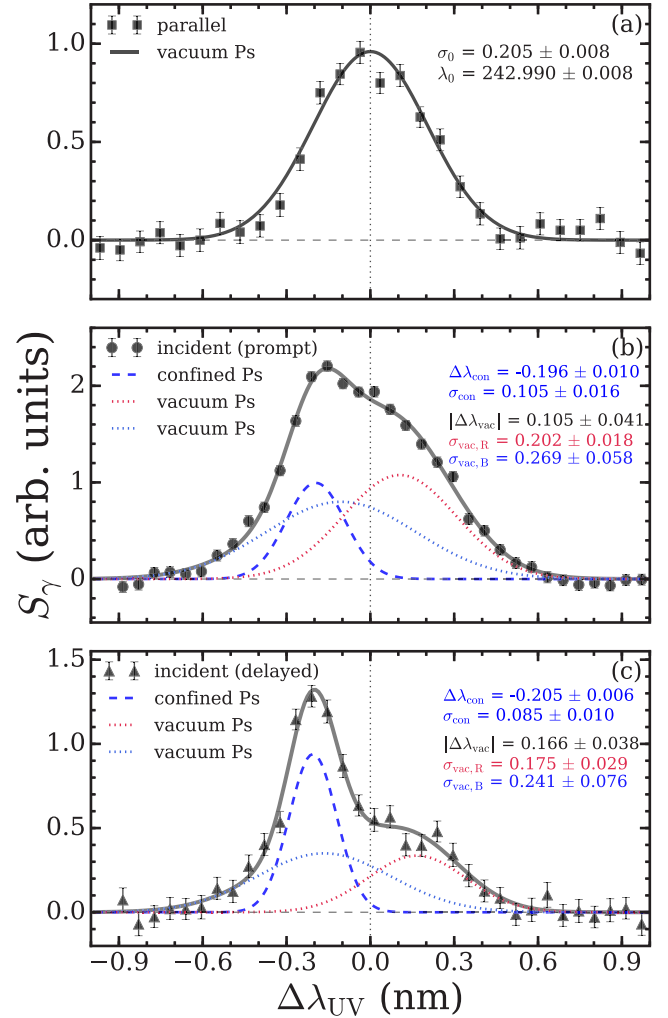

FIG. 2. Excitation of the $1\,^3S_1 \to 2\,^3P_J$ transition in Ps atoms in vacuum (a) and inside MgO powder (b and c). The prompt (b) and delayed (c) data refer to a 10-ns laser delay, as explained in the text. The solid line in (a) is a single-component Gaussian fit to the data. The solid lines in (b) and (c) are the sum of the confined (dashed curves) and vacuum (dotted curves) Gaussian fits with the centroid shifts ($\Delta\lambda_{con/vac}$) relative to the parallel centroid wavelength λ_0 and sigma values ($\sigma_{con/vac}$) indicated in the legends. In (b) and (c) two vacuum curves are required to account for the different Doppler shifts of the incident and reflected laser beams.

a blueshifted peak is also present, arising from vacuum Ps moving in the same direction as reflected laser light.

The blueshifted vacuum peak is not directly observed because it is obscured by a larger peak (also blueshifted) arising from the excitation of confined Ps, which is expected to comprise Dicke-narrowed lines with a distribution of shifts [52]. The measured line shapes were modeled using a single Gaussian function for the parallel case [Fig. 2(a)] and a three-component Gaussian function when the lasers were directed into the target. For the latter case the vacuum peaks were constrained to have equal and opposite shifts but independent amplitudes and widths. The width of the redshifted vacuum peak in Fig. 2(c) (i.e., $\sigma_{vac,R}$) is narrower than the transverse vacuum width [Fig. 2(a)], since the incident laser light does

not interact with the entire angular spread of the Ps atoms. The blueshifted vacuum peak width (i.e., $\sigma_{vac,B}$) is larger than that of the corresponding redshifted peak and is close to the transverse vacuum peak width, suggesting that the reflected laser light is more diffuse than the incident beam. The blueshifted peak corresponding to confined Ps is considerably narrower than the parallel vacuum case, but this width is not representative of Doppler broadening [29].

Similar spectra have been previously observed for Ps atoms excited in mesoporous silica films [52]. In that work the $1\,^3S_1 \rightarrow 2\,^3P_J$ excitation frequency was found to shift by ≈ 100 GHz when atoms were probed inside a mesoporous film. This shift was attributed to the effect of Ps confinement in ≈ 5-nm-diameter voids [53,54]. However, subsequent theoretical analysis has indicated that this interpretation might not be correct [55,56].

The present results, in which the observed $1\,^3S_1 \rightarrow 2\,^3P_J$ shift is equivalent to ≈ 1000 GHz, cannot be explained by confinement effects because the MgO voids are large (on the micron scale) and shifts due to confinement would fall off approximately with the cube of the void radius [56]. As discussed below, we attribute the present results to a resonant interaction with MgO PL absorption bands. Since SiO$_2$ also exhibits strong absorption bands overlapping 243 nm (e.g., [57]), the previously observed shifts may have been caused by the same mechanism(s). In the mesoporous silica measurements [52], only the $1\,^3S_1 \rightarrow 2\,^3P_J$ transition was probed. This measurement provides only the value of the interval and cannot provide any information regarding the individual energy levels. Here we have also measured transitions to several Rydberg levels, which allows us to obtain more information.

Figure 3 shows $2\,^3P_J \rightarrow 11\,^3S/11\,^3D$ excitation spectra, measured both in vacuum and inside the MgO sample. These data were recorded in the same way as the data shown in Fig. 2, except the IR wavelength was scanned while the UV wavelength was fixed at $\lambda = 243$ nm or $\lambda = 242.8$ nm for vacuum or confined excitation, respectively (see Fig. 2). The vacuum Rydberg transitions were found to occur at the expected IR wavelengths [58]. For Ps excited with the lasers directed into the target [Figs. 3(b) and 3(c)], however, we again observe a large blueshifted peak and a smaller redshifted peak with respect to the vacuum IR laser wavelengths.

The blueshifted UV laser wavelength preferentially excited *vacuum* Ps that is moving away from the UV laser. Since the IR and UV lasers propagate in opposite directions, however, these atoms will be moving towards the IR laser. Therefore, IR excitation of these atoms will be redshifted with respect to the IR laser wavelength. The redshifted IR vacuum peak thus confirms that there is indeed a component of blueshifted UV excitation, justifying the three-component Gaussian fit used in Figs. 2(b) and 2(c). For the data in Figs. 3(b) and 3(c), however, a two-component fit was used, since the blue-detuned UV laser will not produce any $n = 2$ atoms that the blue-detuned IR laser can excite.

The data in Figs. 2 and 3 show that Ps atoms can be excited to $n = 2$ and to Rydberg levels inside the MgO, and that both the $1\,^3S_1 \rightarrow 2\,^3P_J$ and the $2\,^3P_J \rightarrow n\,^3D/n\,^3S$ intervals are increased relative to the corresponding vacuum transitions. Since Rydberg states are observed by virtue of their long lifetimes [39], these data also show that, despite numerous
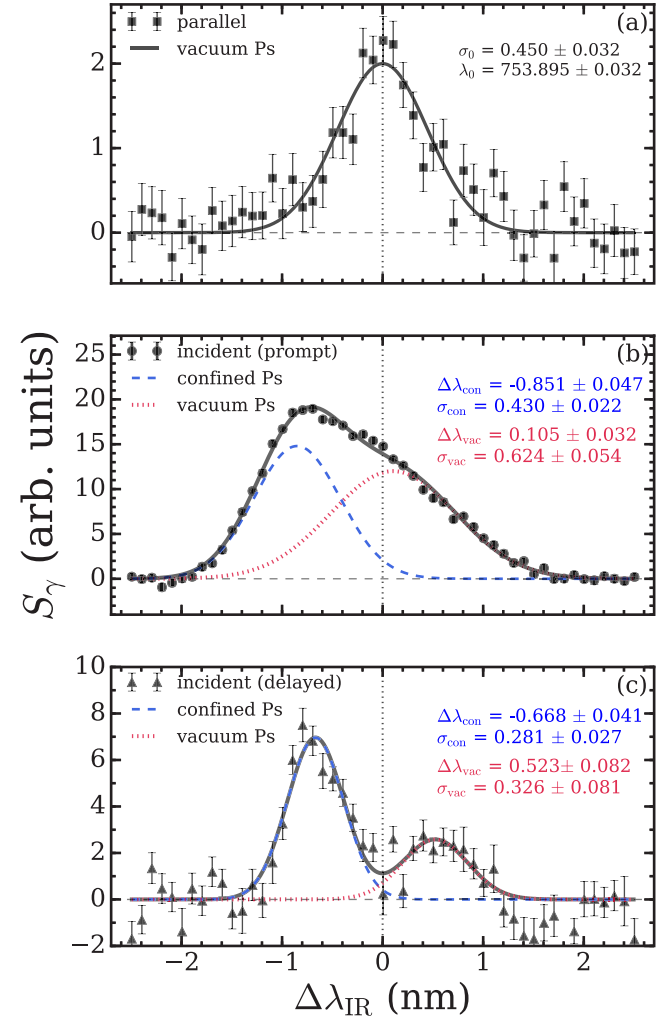

FIG. 3. Excitation of the $2\,^3P_J \rightarrow 11\,^3S/11\,^3D$ transition in Ps atoms in vacuum (a) and inside MgO powder (b and c). The prompt (b) and delayed (c) data refer to the laser delay, as explained in the text. The solid line in (a) is a single-component Gaussian fit to the data. The solid lines in (b) and (c) are the sum of the confined (dashed curves) and vacuum (dotted curves) Gaussian fits with the centroid shifts ($\Delta\lambda_{con/vac}$) relative to the parallel centroid wavelength λ_0 and sigma values ($\sigma_{con/vac}$) indicated in the legends.

collisions with MgO surfaces, the Rydberg Ps atoms are not deexcited and are able to leave the sample.

Rydberg atoms are highly sensitive to external fields and other interactions [59], so it is perhaps not surprising that transitions to Rydberg levels inside the MgO target are shifted. However, by recording spectra covering many transitions we find that the Rydberg levels are shifted by an amount that does *not* depend on the principal quantum number of the final state. This can be seen explicitly in Fig. 4, which shows $2\,^3P_J \rightarrow n\,^3S/n\,^3D$ transitions (recorded using the UV wavelength indicated in each panel) for n ranging from 10 up to the ionization limit; any Rydberg level shift would be expected to scale strongly with n, at least with n^2, and possibly faster [59]. Superficially, the form of the line shapes in Fig. 4 are similar to Fano profiles [60], which exhibit asymmetric effects through interference phenomena (see, e.g., [61]). However, as can be
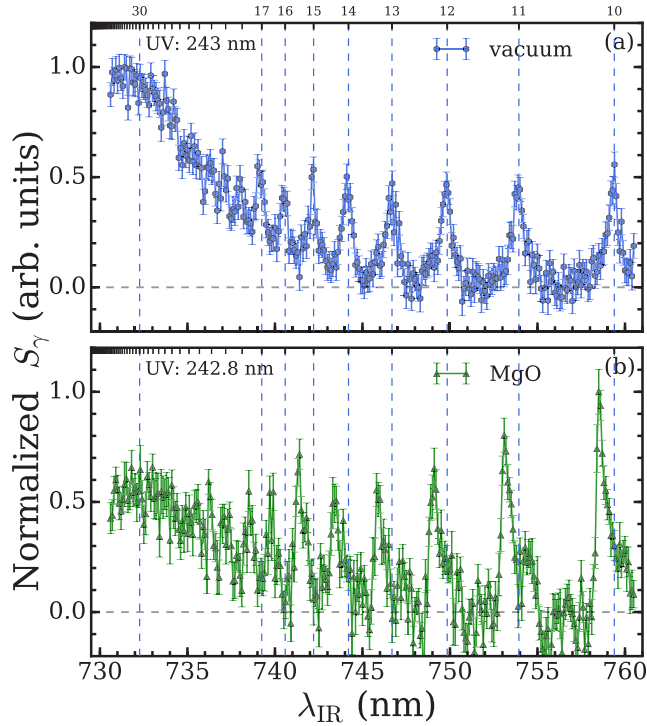
FIG. 4. Excitation of Rydberg Ps atoms (a) in vacuum and (b) inside the MgO smoke powder target (see Fig. 1). The principal quantum numbers of the Rydberg levels are indicated by the dashed vertical lines and at the top of the figure.
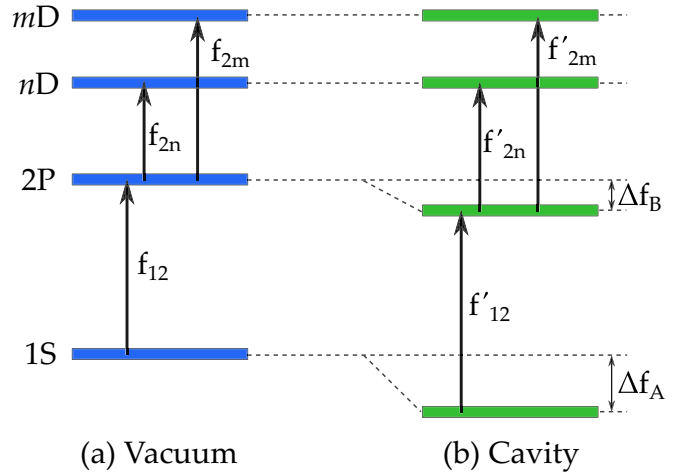

FIG. 5. Schematic representation of Ps energy levels (a) in vacuum and (b) in the MgO powder inferred from the observed transition intervals. Here f_{12} and f'_{12} refer to confined and vacuum transitions (from $n = 1$ to $n = 2$), respectively. Similarly, $f_{2n(m)}$ and $f'_{2n(m)}$ refer to confined and vacuum transitions from $n = 2$ to levels with principal quantum number $n(m)$, respectively.

seen explicitly in Fig. 3, this apparent asymmetry is actually due to the Doppler-shifted component of the spectrum. We are only able to resolve states up to $n \approx 17$ because of the laser bandwidth and Doppler broadening effects [37]. Nevertheless, the data clearly show a near constant offset from the expected wavelengths for the confined Rydberg transitions.

When measuring the interval for only one transition (as in [52]), there is no way to know if individual levels are shifted. By measuring multiple Rydberg transitions, however, it is possible to probe effects associated with particular levels. In the present data it is immediately evident that the $n = 2$ level is shifted but the Rydberg levels are not. Moreover, since the energy shift of these transitions is not the same as that observed for the $1\,^3S_1 \rightarrow 2\,^3P_J$ interval, we can conclude that the $n = 1$ level is also shifted. Our interpretation of the MgO-induced level shifts is indicated schematically in Fig. 5. The fact that the Rydberg levels are apparently unaffected is taken to be evidence that the underlying mechanism giving rise to these effects proceeds via interactions involving only the $1\,^3S_1$ and $2\,^3P_J$ levels.

The shift of the $n = 2$ level, Δf_B, can be associated with the difference between vacuum and confined Rydberg transitions: i.e., $\Delta f_B = f_{2n} - f'_{2n}$. Fitting all transitions in the range $n = 10$–17 in the same way as shown in Fig. 3 gives an average wavelength shift of 0.702 ± 0.017 nm [see Fig. 6(a)], corresponding to $\Delta f_B = 365 \pm 10$ GHz. The ground-state shift, Δf_A, can be written as $\Delta f_A = f'_{12} - f_{12} - \Delta f_B$. From Fig. 2 we find that $f'_{12} - f_{12} = 1046 \pm 60$ GHz, so that $\Delta f_A = 690 \pm 65$ GHz. To highlight the constant shift of

Rydberg levels, the data of Fig. 4 have been plotted in Fig. 6 as a function of IR photon energy, with the confined Rydberg data shifted by 1.6 meV.

The observation that the Rydberg levels are not shifted indicates that the MgO target is not charging up and producing large electric fields during the experiments; such fields would have a significant effect on any highly excited Rydberg states [62]. We also note that during the course of long measurements no instabilities in the positron beam were observed, which also indicates that no significant charging occurred. It is worth noting that this is by no means an obvious outcome in experiments in which an insulator is irradiated with both positron and UV light pulses. One possible explanation for this observation could be that the negative electron affinity of MgO [63] causes electrons to leave the sample rather than accumulate on surfaces.

Our data show conclusively that the mechanism underlying the observed shifts involves only the lower-lying Ps energy levels (i.e., $n = 1$ and $n = 2$) and not the higher-lying Rydberg levels. At the same time, it is well known that MgO has strong PL absorption bands that overlap with the $1\,^3S_1 \rightarrow 2\,^3P_J$ transition in Ps. In MgO absorption may occur over a range of ≈ 230–255 nm [64], although significant variations may exist that depend on the details of the MgO production and structure. Thus, it appears that resonant interactions between Ps atoms and the same molecular states that give rise to MgO photoluminescence are responsible for the observed Ps energy-level shifts. The PL effects in MgO are primarily surface phenomena [38,65,66], which means that Ps collisions with nanocrystal surfaces necessarily involve interactions with the MgO surface states that absorb light at the same wavelength as $1\,^3S_1 \rightarrow 2\,^3P_J$ transitions.

To obtain a qualitative understanding of the observed shifts, we consider the effect of resonant electric dipole-dipole interactions between the Ps atoms and the MgO [67,68]; since the $1\,^3S_1$ and $2\,^3P_J$ levels exhibit different frequency shifts in
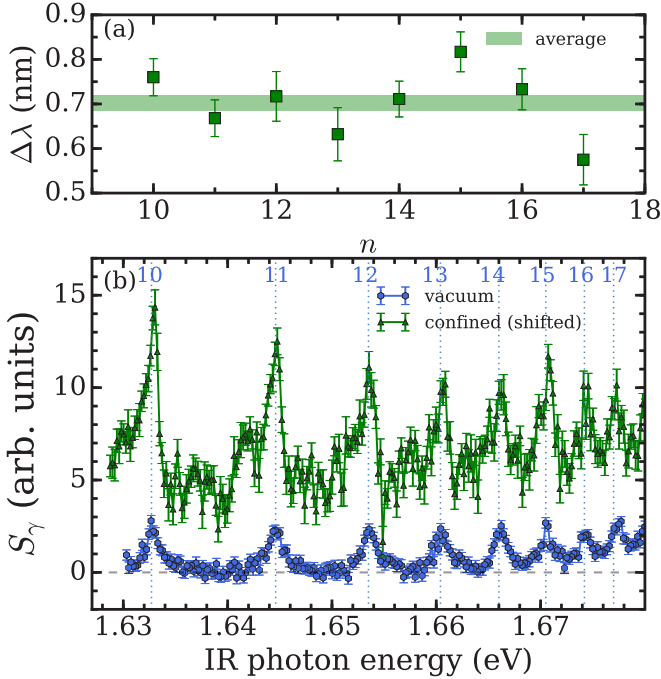
FIG. 6. (a) Observed shift of Rydberg transitions relative to vacuum measurements and (b) confined and vacuum spectra plotted as a function of the IR photon energy. The mean shifts were obtained using the procedure described in the text (see also Fig. 4). The confined spectrum in (b) is shifted by an amount equivalent to a wavelength shift of 0.7 nm ($\approx$1.6 meV), the mean measured shift of all the data as shown in (a).

the experiments (i.e., -690 and -365 GHz, respectively) the interaction between the atoms and the MgO must also include at least one additional Ps energy level. To account for this we employ a simple model in which we treat the Ps atom, neglecting contributions from fine- and hyperfine structure, as a three-level system composed of the bound $1s$ and $2p$ states, and the d continuum, 243 nm above the $2p$ state, i.e., 3.4 eV ($\equiv$822 THz) above the ionization limit, as depicted in Fig. 7(a). To further simplify this analysis we neglect the s continuum, since the $2p \rightarrow s$ (continuum) transition is approximately 5 times weaker than the $2p \rightarrow d$ (continuum) transition.

In this system the $1s \rightarrow 2p$ transition couples resonantly to the 243-nm component of the MgO photoabsorption spectrum, as does the $2p \rightarrow d$ (continuum) transition. The resonant dipole-dipole interaction between the Ps atoms and the MgO nanocrystals can then be estimated by approximating the interaction energy, neglecting the angular dependence [67], for each individual resonance as

$$V_{dd} = \frac{d_{Ps}\, d_{MgO}}{4\pi\, \epsilon_0 R_{Ps-MgO}^3}, \tag{1}$$

where ϵ_0 is the vacuum permittivity, and R_{Ps-MgO} is the distance between the Ps atom and a single MgO absorber. Here "MgO absorber" refers an individual nanocrystal surface feature, such as an edge, kink, defect, or terrace [64], and not to a single MgO molecule.
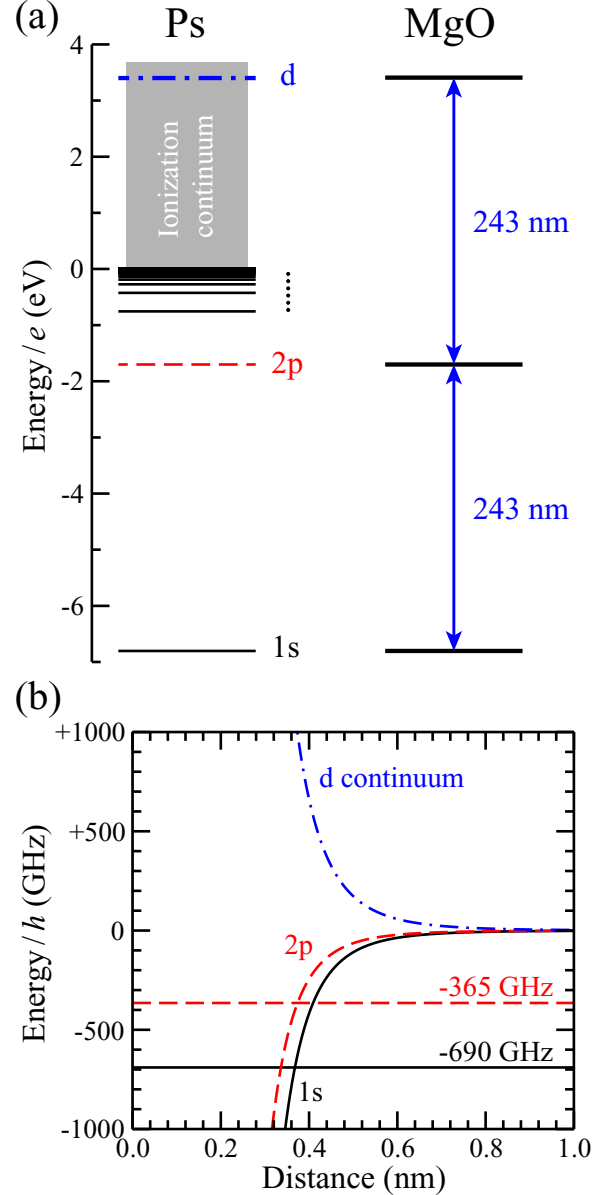

FIG. 7. (a) Diagram of the energy-level structure in Ps and the corresponding 243-nm transitions in MgO between which the resonant dipole-dipole interactions are considered. (b) Dependence of the frequency shifts of the bound $1s$ (continuous black curve) and $2p$ (dashed red curve) states and the d continuum (dash dotted curve) in Ps on the distance from a single MgO absorber with a resonance at 243 nm and $\Delta\lambda = 23.5$ nm, as determined from the measured shifts of the $1s$ and $2s$ states.

The $1s \rightarrow 2p$ transition dipole moment in Ps is $d_{1s-2p} = 0.74\, e\, a_{Ps}$, while the corresponding transition dipole moment of an MgO absorber is estimated to be $d_{MgO-MgO^*} \approx 1\, e\, a_0$ [64], where e is the electronic charge and a_0 ($a_{Ps} = 2a_0$) is the Bohr radius (Ps Bohr radius). In the treatment of the dipole-dipole interaction involving the transition from the bound $2p$ state to the continuum in Ps, and the MgO, it is necessary to consider the extent of the continuum over which the coupling occurs. Since the absorption of MgO at wavelengths close to 243 nm covers the range from $\sim$230 to $\sim$255 nm, the

electric dipole moments for the $2p$ to continuum transition in Ps, and the MgO $\rightarrow$ MgO* transition to which it couples, was determined by integrating over a wavelength range $\Delta\lambda$ in each case. Considering a Ps $2p$ to continuum transition moment per unit wavelength, determined by extrapolation of transitions to the bound nd Rydberg series [69] of $0.002 \, e \, a_{Ps}$ nm^{-1}, and an MgO transition moment per unit wavelength of $1 \, e \, a_0$ nm^{-1}, the value of $\Delta\lambda$ required to obtain a ratio of the frequency shifts of the $2 \,^3P$ and $2 \,^3S_1$ levels of $365/690 = 0.53$ as observed in the experiments was 23.5 nm. This resulted in values of d_{2p-d} and $d_{MgO-MgO^*}$ of $0.05 \, e \, a_{Ps}$ and $23.5 \, e \, a_0$, respectively. As can be seen from Fig. 7(b), the resonant electric dipole-dipole coupling in this model three-level Ps atom with a single MgO absorber yields the observed frequency shifts of the $1s$ and $2p$ states (-690 and -365 GHz, respectively) for an atom-surface distance of 0.37 nm. Because the transitions from the $2 \,^3P$ state to the Rydberg states do not overlap with the resonances in the MgO absorption spectrum, these transitions do not undergo resonant dipole-dipole interactions with the MgO, and the observed shift of $2 \,^3P \rightarrow n \,^3S/n \,^3D$ transition frequencies in the experiments does not exhibit a measurable n dependence.

The atom-surface distances obtained using this simple model that give rise to the experimentally observed Ps frequency shifts are on the scale of the size of the excited $2 \,^3P$ Ps atoms ($\sim$0.5 nm). This distance is very small compared to the size of the open volumes in the MgO powder [see Fig. 1(b)], and there is no reason to expect atoms to become localized near the nanocrystal surfaces. Furthermore, since the Rydberg levels are not shifted, these atoms must in general be further away than the Rydberg atom size, which is approximately 40 nm for $n = 17$ Ps. Therefore we conclude that Ps atoms interact collectively with a large number of MgO absorbers over length scales on the order of 100 nm. A collective coupling of this sort would increase the magnitude of the effective MgO $\rightarrow$ MgO* electric dipole transition moments, increasing the resulting frequency shifts of the Ps energy levels at any particular value of R_{Ps-MgO}.

It would be of interest to optically probe Ps atoms emitted from single-crystal MgO and SiO$_2$ surfaces directly into vacuum [70], and also in large cubic internal voids generated by ion implantation and subsequent annealing [71], to further clarify the nature of Ps-surface interactions and associated energy-level shifts. Other effects such as confinement or collisions would in general affect Rydberg levels much more strongly than the lower-lying levels and can therefore be ruled out as the mechanism behind the large observed shifts. This does not mean, however, that the Rydberg states are entirely unaffected by their environment; for example, experiments with Rydberg Na atoms passing through metal plates with micron separations have shown van der Waals energy shifts on the 100 MHz level [72] which, if present, would not be observable in our experiments.

While properly engineered insulating structures are undoubtedly useful to create and confine Ps atoms at high densities [73], the effects we have described here could preclude those same structures from being used to optically study or manipulate dense Ps ensembles. For example, time-delayed single-photon Doppler measurements could in principal be used to measure Ps cooling rates in cavities large enough to avoid line narrowing. Similarly, laser cooling in such cavities might then also be possible. However, large shifts as we have observed would not be compatible with any optical methods that rely on probing Doppler profiles. PL absorption bands in the deep UV are common to many insulating materials that are useful for Ps formation, including mesoporous SiO$_2$ [57]. This does not necessarily mean that there are no viable alternative materials, but it could inform fabrication processes if different ways of producing such materials impact the PL properties differently, in particular, regarding surface-based effects. It may be possible to perform optical characterization of Ps in the presence of resonant shifts, although this will complicate the interpretation of such data.

The ability to measure Ps properties in various experimental environments will be critical for future experiments involving high-density Ps, such as studies of Ps$_2$ molecules [74], and to continue progress towards Ps BEC along the lines suggested by Platzman and Mills [13,17]. An optical measurement of the temperature of dense Ps confined in a cavity is probably not possible due to line narrowing [29], but the angular correlation of two-photon Ps annihilation radiation can be used [75].

A direct measurement of the Ps density would be a critical diagnostic for any experiments involving Ps-Ps interactions. In this case the density of a confined Ps ensemble can, in principle, be inferred from measured scattering rates [76–78]: if Ps is generated in a known geometry, then the density can be determined from changes in the mean Ps lifetime arising from spin exchanging collisions, for which the scattering cross sections have been calculated [79]. However, such measurements rely on an asymmetry between spin states, and once the minority spin component has been depleted, this signal will disappear. It would, therefore, be beneficial to have an independent density measurement that does not require Ps polarization. This could be achieved spectroscopically by measuring the collisional frequency (or clock) shift [80], as has been done for trapped hydrogen [34]. The calculation of Higgins *et al.* [35] indicates that for Ps the clock shift will be $\approx 1 \times 10^{-7}$ Hz cm^3 (for hydrogen this has been measured to be 3.8×10^{-10} Hz cm^{-3}). Thus, for a Ps density of 10^{16} cm^3 (cf. [77]) we would expect a shift on the order of 1 GHz. The natural linewidth of the $1 \,^3S_1 \rightarrow 2 \,^3S_1$ transition is 1.3 MHz [20], meaning that a clock shift bigger than a few megahertz would be very apparent under most conditions. Since the $1 \,^3S_1 \rightarrow 2 \,^3S_1$ transition proceeds via the absorption of two 486-nm photons, the laser light would not be resonant with PL absorption in MgO or SiO$_2$, and there may not be any large shift of the type we have observed here. However, this cannot be established with certainty until the mechanism underlying the shift has been fully evaluated.

IV. CONCLUSIONS

We have observed shifts of the $n = 1$ and $n = 2$ energy levels of Ps atoms while they are inside the internal voids of MgO smoke powder. Measurements of a series of Rydberg transitions indicate that these energy shifts affect only the lower-lying levels, which we attribute to resonant interactions

between these Ps levels and overlapping MgO PL absorption bands. Since such UV PL properties are very common in materials that are suitable for Ps confinement, similar shifts can be expected in other useful Ps forming materials as well [81]. The existence of these shifts could affect attempts to employ spectroscopic characterization and control (particularly laser cooling) of confined Ps, which are required for the optimization of experiments involving high-density Ps ensembles. Thus, it may be necessary to develop alternative materials suitable for both Ps confinement and optical probes [82].

[1] S. Chu, L. Hollberg, J. E. Bjorkholm, A. Cable, and A. Ashkin, Three-Dimensional Viscous Confinement and Cooling of Atoms by Resonance Radiation Pressure, Phys. Rev. Lett. **55**, 48 (1985).

[2] E. L. Raab, M. Prentiss, A. Cable, S. Chu, and D. E. Pritchard, Trapping of Neutral Sodium Atoms with Radiation Pressure, Phys. Rev. Lett. **59**, 2631 (1987).

[3] I. D. Setija, H. G. C. Werij, O. J. Luiten, M. W. Reynolds, T. W. Hijmans, and J. T. M. Walraven, Optical Cooling of Atomic Hydrogen in a Magnetic Trap, Phys. Rev. Lett. **70**, 2257 (1993).

[4] C. R. Monroe, E. A. Cornell, C. A. Sackett, C. J. Myatt, and C. E. Wieman, Measurement of Cs-Cs Elastic Scattering at $T = 30\,\mu$K, Phys. Rev. Lett. **70**, 414 (1993).

[5] A. G. Martin, K. Helmerson, V. S. Bagnato, G. P. Lafyatis, and D. E. Pritchard, rf Spectroscopy of Trapped Neutral Atoms, Phys. Rev. Lett. **61**, 2431 (1988).

[6] M. H. Anderson, J. R. Ensher, M. R. Matthews, C. E. Wieman, and E. A. Cornell, Observation of Bose-Einstein condensation in a dilute atomic vapor, Science **269**, 198 (1995).

[7] C. E. Wieman, D. E. Pritchard, and D. J. Wineland, Atom cooling, trapping, and quantum manipulation, Rev. Mod. Phys. **71**, S253 (1999).

[8] A. J. Leggett, Bose-Einstein condensation in the alkali gases: Some fundamental concepts, Rev. Mod. Phys. **73**, 307 (2001).

[9] S. C. Doret, C. B. Connolly, W. Ketterle, and J. M. Doyle, Buffer-Gas Cooled Bose-Einstein Condensate, Phys. Rev. Lett. **103**, 103005 (2009).

[10] J. Hu, A. Urvoy, Z. Vendeiro, V. Crépel, W. Chen, and V. Vuletić, Creation of a Bose-condensed gas of ^{87}Rb by laser cooling, Science **358**, 1078 (2017).

[11] D. G. Fried, T. C. Killian, L. Willmann, D. Landhuis, S. C. Moss, D. Kleppner, and T. J. Greytak, Bose-Einstein Condensation of Atomic Hydrogen, Phys. Rev. Lett. **81**, 3811 (1998).

[12] E. P. Liang and C. D. Dermer, Laser cooling of positronium, Opt. Commun. **65**, 419 (1988).

[13] P. M. Platzman and A. P. Mills, Jr., Possibilities for Bose condensation of positronium, Phys. Rev. B **49**, 454 (1994).

[14] M. Bertolotti and C. Sibilia, Coherent γ-emission by stimulated annihilation of electron-positron pairs, Appl. Phys. **19**, 127 (1979).

[15] Y.-H. Wang, B. M. Anderson, and C. W. Clark, Spinor Bose-Einstein condensates of positronium, Phys. Rev. A **89**, 043624 (2014).

[16] H. K. Avetissian, A. K. Avetissian, and G. F. Mkrtchian, Self-Amplified Gamma-Ray Laser on Positronium Atoms from a Bose-Einstein Condensate, Phys. Rev. Lett. **113**, 023904 (2014).

[17] A. P. Mills, Jr., Physics with many positrons, in *Course CLXXIV "Physics with Many Positrons,"* edited by R. S. Brusa, A. Dupasquier, and A. P. Mills, Jr., Proceedings of the International School of Physics "Enrico Fermi" (IOS Press, Amsterdam, 2010), pp. 77–187.

[18] C. Pethick and H. Smith, *Bose-Einstein Condensation in Dilute Gases* (Cambridge University Press, Cambridge, UK, 2002).

[19] A. Ore and J. L. Powell, Three-photon annihilation of an electron-positron pair, Phys. Rev. **75**, 1696 (1949).

[20] D. B. Cassidy, Experimental progress in positronium laser physics, Eur. Phys. J. D **72**, 53 (2018).

[21] B. S. Cooper, J.-P. Boilot, C. Corbel, F. Guillemot, L. Gurung, L. Liszkay, and D. B. Cassidy, Annihilation of positronium atoms confined in mesoporous and macroporous SiO$_2$ films, Phys. Rev. B **97**, 205302 (2018).

[22] H. Saito and T. Hyodo, Quenching of positronium by surface paramagnetic centers in ultraviolet- and positron-irradiated fine oxide grains, Phys. Rev. B **60**, 11070 (1999).

[23] D. W. Gidley, H. G. Peng, and R. S. Vallery, Positron annihilation as a method to characterize porous materials, Annu. Rev. Mater. Res. **36**, 49 (2006).

[24] O. Morandi, P.-A. Hervieux, and G. Manfredi, Bose-Einstein condensation of positronium in silica pores, Phys. Rev. A **89**, 033609 (2014).

[25] K. Shu, X. Fan, T. Yamazaki, T. Namba, S. Asai, K. Yoshioka, and M. Kuwata-Gonokami, Study on cooling of positronium for Bose Einstein condensation, J. Phys. B: At. Mol. Opt. Phys. **49**, 104001 (2016).

[26] C. He, S. Wang, Y. Kobayashi, T. Ohdaira, and R. Suzuki, Role of pore morphology in positronium diffusion in mesoporous silica thin films and in positronium emission from the surfaces, Phys. Rev. B **86**, 075415 (2012).

[27] H. Saito and T. Hyodo, Cooling and quenching of positronium in porous material, in *New Directions in Antimatter Chemistry and Physics*, edited by C. M. Surko and F. A. Gianturco (Springer, Netherlands, Dordrecht, 2001), pp. 101–114.

[28] T. Kumita, T. Hirose, M. Irako, K. Kadoya, B. Matsumoto, K. Wada, N. N. Mondal, H. Yabu, K. Kobayashi, and M. Kajita, Study on laser cooling of ortho-positronium, Nucl. Instrum. Methods Phys. Res. Sect. B **192**, 171 (2002).

[29] R. H. Dicke, The effect of collisions upon the Doppler width of spectral lines, Phys. Rev. **89**, 472 (1953).

[30] R. P. Frueholz and J. C. Camparo, Implications of the trapping-desorption and direct inelastic-scattering channels on Dicke-narrowed line shapes, Phys. Rev. A **35**, 3768 (1987).

[31] C. I. Westbrook, R. N. Watts, C. E. Tanner, S. L. Rolston, W. D. Phillips, P. D. Lett, and P. L. Gould, Localization of Atoms in

a Three-Dimensional Standing Wave, Phys. Rev. Lett. **65**, 33 (1990).

[32] D. Kielpinski, Laser cooling of atoms and molecules with ultrafast pulses, Phys. Rev. A **73**, 063407 (2006).

[33] J. P. Bartolotta, M. A. Norcia, J. R. K. Cline, J. K. Thompson, and M. J. Holland, Laser cooling by sawtooth-wave adiabatic passage, Phys. Rev. A **98**, 023404 (2018).

[34] T. C. Killian, D. G. Fried, L. Willmann, D. Landhuis, S. C. Moss, T. J. Greytak, and D. Kleppner, Cold Collision Frequency Shift of the $1S$- $2S$ Transition in Hydrogen, Phys. Rev. Lett. **81**, 3807 (1998).

[35] M. D. Higgins, K. M. Daily, and C. H. Greene, Low-energy scattering properties of ground-state and excited-state positronium collisions, Phys. Rev. A **100**, 012711 (2019).

[36] K. P. Ziock, R. H. Howell, F. Magnotta, R. A. Failor, and K. M. Jones, First Observation of Resonant Excitation of High-n States in Positronium, Phys. Rev. Lett. **64**, 2366 (1990).

[37] D. B. Cassidy, T. H. Hisakado, H. W. K. Tom, and A. P. Mills, Jr., Efficient Production of Rydberg Positronium, Phys. Rev. Lett. **108**, 043401 (2012).

[38] S. Coluccia, A. M. Deane, and A. J. Tench, Photoluminescent spectra of surface states in alkaline earth oxides, J. Chem. Soc. Faraday Trans. 1 **74**, 2913 (1978).

[39] B. S. Cooper, A. M. Alonso, A. Deller, T. E. Wall, and D. B. Cassidy, A trap-based pulsed positron beam optimised for positronium laser spectroscopy, Rev. Sci. Instrum. **86**, 103101 (2015).

[40] A. M. Alonso, B. S. Cooper, A. Deller, and D. B. Cassidy, Single-shot positron annihilation lifetime spectroscopy with LYSO scintillators, Nucl. Instrum. Methods Phys. Res. Sect. A **828**, 163 (2016).

[41] R. Paulin and G. Amrosino, Annihilation libre de l'ortho-positonium formé dans certaines poudres de grande surface spécifique, J. Phys. France **29**, 263 (1968).

[42] D. B. Cassidy, S. H. M. Deng, H. K. M. Tanaka, and A. P. Mills, Jr., Single shot positron annihilation lifetime spectroscopy, Appl. Phys. Lett. **88**, 194105 (2006).

[43] D. B. Cassidy and A. P. Mills, Jr., A fast detector for single-shot positron annihilation lifetime spectroscopy, Nucl. Instrum. Methods Phys. Res. Sect. A **580**, 1338 (2007).

[44] A. Deller, A. M. Alonso, B. S. Cooper, S. D. Hogan, and D. B. Cassidy, Measurement of Rydberg positronium fluorescence lifetimes, Phys. Rev. A **93**, 062513 (2016).

[45] A. F. Moodie and C. E. Warble, Electron microscopic investigations of MgO morphology and surfaces, J. Cryst. Growth **10**, 26 (1971).

[46] C. F. Jokes, R. L. Segall, R. St. C. Smart, and P. S. Turner, Size distribution of MgO smoke particles, Philos. Mag. A **42**, 267 (1980).

[47] C. A. Schneider, W. S. Rasband, and K. W. Eliceiri, NIH image to imageJ: 25 years of image analysis, Nat. Methods **9**, 671 (2012).

[48] L. Gurung, A. M. Alonso, T. J. Babij, B. S. Cooper, A. L. Shluger, and D. B. Cassidy, Positronium emission from MgO smoke nanocrystals, J. Phys. B: At. Mol. Opt. Phys. **52**, 105004 (2019).

[49] Y. Nagashima, M. Kakimoto, T. Hyodo, K. Fujiwara, A. Ichimura, T. Chang, J. Deng, T. Akahane, T. Chiba, K. Suzuki, B. T. A. McKee, and A. T. Stewart, Thermalization of free positronium atoms by collisions with silica-powder grains,

[50] aerogel grains, and gas molecules, Phys. Rev. A **52**, 258 (1995).

[50] A. Deller, B. S. Cooper, T. E. Wall, and D. B. Cassidy, Positronium emission from mesoporous silica studied by laser-enhanced time-of-flight spectroscopy, New J. Phys. **17**, 043059 (2015).

[51] W. Demtröder, *Laser Spectroscopy*, 3rd ed. (Springer, New York, 2003).

[52] D. B. Cassidy, M. W. J. Bromley, L. C. Cota, T. H. Hisakado, H. W. K. Tom, and A. P. Mills, Jr., Cavity Induced Shift and Narrowing of the Positronium Lyman-α Transition, Phys. Rev. Lett. **106**, 023401 (2011).

[53] D. B. Cassidy, P. Crivelli, T. H. Hisakado, L. Liszkay, V. E. Meligne, P. Perez, H. W. K. Tom, and A. P. Mills, Jr., Positronium cooling in porous silica measured via Doppler spectroscopy, Phys. Rev. A **81**, 012715 (2010).

[54] P. Crivelli, U. Gendotti, A. Rubbia, L. Liszkay, P. Perez, and C. Corbel, Measurement of the orthopositronium confinement energy in mesoporous thin films, Phys. Rev. A **81**, 052703 (2010).

[55] D. G. Green and G. F. Gribakin, Comment on "Cavity Induced Shift and Narrowing of the Positronium Lyman-α Transition," Phys. Rev. Lett. **106**, 209301 (2011).

[56] R. Brown, Q. Prigent, A. R. Swann, and G. F. Gribakin, Effective radius of ground- and excited-state positronium in collisions with hard walls, Phys. Rev. A **95**, 032705 (2017).

[57] A. Anedda, C. M. Carbonaro, F. Clemente, R. Corpino, and P. C. Ricci, Mesoporous silica photoluminescence properties in samples with different pore size, Mater. Sci. Eng.: C **23**, 1073 (2003).

[58] T. E. Wall, A. M. Alonso, B. S. Cooper, A. Deller, S. D. Hogan, and D. B. Cassidy, Selective Production of Rydberg-Stark States of Positronium, Phys. Rev. Lett. **114**, 173001 (2015).

[59] T. F. Gallagher, *Rydberg Atoms* (Cambridge University Press, Cambridge, UK, 1994).

[60] U. Fano, Effects of configuration interaction on intensities and phase shifts, Phys. Rev. **124**, 1866 (1961).

[61] S. Schippers, A. M. ller, B. M. McLaughlin, A. Aguilar, C. Cisneros, E. D. Emmons, M. F. Gharaibeh, and R. A. Phaneuf, Photoionization studies of the b valence shell: Experiment and theory, J. Phys. B: At. Mol. Opt. Phys. **36**, 3371 (2003).

[62] A. Osterwalder and F. Merkt, Using High Rydberg States as Electric Field Sensors, Phys. Rev. Lett. **82**, 1831 (1999).

[63] H. Rougeot and C. Baud, *Negative Electron Affinity Photoemitters* (Academic Press, New York, 1979), pp. 1–36.

[64] C. Chizallet, G. Costentin, H. Lauron-Pernot, J.-M. Krafft, M. Che, F. Delbecq, and P. Sautet, Assignment of photoluminescence spectra of MgO powders: TD-DFT cluster calculations combined to experiments. Part II. Hydroxylation effects, J. Phys. Chem. C **112**, 19710 (2008).

[65] A. J. Tench and G. T. Pott, Surface states in some alkaline earth oxides, Chem. Phys. Lett. **26**, 590 (1974).

[66] S. Coluccia, A. J. Tench, and R. L. Segall, Surface structure and surface states in magnesium oxide powders, J. Chem. Soc. Faraday Trans. 1 **75**, 1769 (1979).

[67] T. F. Gallagher, Resonant collisional energy transfer between Rydberg atoms, Phys. Rep. **210**, 319 (1992).

[68] T. F. Gallagher and P. Pillet, Dipole-dipole interactions of Rydberg atoms, Adv. At. Mol. Opt. Phys. **56**, 161 (2008).

[69] U. Fano and J. W. Cooper, Spectral distribution of atomic oscillator strengths, Rev. Mod. Phys. **40**, 441 (1968).

[70] Y. Nagashima, Y. Morinaka, T. Kurihara, Y. Nagai, T. Hyodo, T. Shidara, and K. Nakahara, Origins of positronium emitted from SiO$_2$, Phys. Rev. B **58**, 12676 (1998).

[71] S. W. H. Eijt, C. V. Falub, A. van Veen, H. Schut, P. E. Mijnarends, M. A. van Huis, and A. V. Fedorov, Ion-implantation generated nanovoids in Si and MgO monitored by high resolution positron beam analysis, MRS Proc. **647**, O14.11/R9.11 (2000).

[72] V. Sandoghdar, C. I. Sukenik, E. A. Hinds, and S. Haroche, Direct Measurement of the van der Waals Interaction Between an Atom and Its Images in a Micron-Sized Cavity, Phys. Rev. Lett. **68**, 3432 (1992).

[73] D. B. Cassidy, S. H. M. Deng, R. G. Greaves, T. Maruo, N. Nishiyama, J. B. Snyder, H. K. M. Tanaka, and A. P. Mills, Jr., Experiments with a High-Density Positronium Gas, Phys. Rev. Lett. **95**, 195006 (2005).

[74] D. B. Cassidy, T. H. Hisakado, H. W. K. Tom, and A. P. Mills, Jr., Optical Spectroscopy of Molecular Positronium, Phys. Rev. Lett. **108**, 133402 (2012).

[75] G. G. Cecchini, A. C. L. Jones, M. Fuentes-Garcia, D. J. Adams, M. Austin, E. Membreno, and A. P. Mills, Jr., Detector for

[76] D. B. Cassidy and A. P. Mills, Jr., Interactions between Positronium Atoms in Porous Silica, Phys. Rev. Lett. **100**, 013401 (2008).

[77] D. B. Cassidy, V. E. Meligne, and A. P. Mills, Jr., Production of a Fully Spin-Polarized Ensemble of Positronium Atoms, Phys. Rev. Lett. **104**, 173401 (2010).

[78] D. B. Cassidy and A. P. Mills, Jr., Enhanced Ps-Ps Interactions due to Quantum Confinement, Phys. Rev. Lett. **107**, 213401 (2011).

[79] I. A. Ivanov, J. Mitroy, and K. Varga, Positronium-positronium scattering using the stochastic variational method, Phys. Rev. A **65**, 022704 (2002).

[80] M. J. Jamieson, A. Dalgarno, and J. M. Doyle, Scattering lengths for collisions of ground state and metastable state hydrogen atoms, Mol. Phys. **87**, 817 (1996).

[81] P. Sen and A. P. Patro, Positron annihilation studies in oxides, Il Nuovo Cimento B (1965-1970) **64**, 324 (1969).

[82] A. P. Mills, Jr., Positronium Bose-Einstein condensation in liquid ^{4}He bubbles, Phys. Rev. A **100**, 063615 (2019).

positronium temperature measurements by two-photon angular correlation, Rev. Sci. Instrum. **89**, 053106 (2018).